

# Radiation Shielding Potentials of Rene Alloys by Phy-X/PSD Code

Z. AYGUN<sup>a,\*</sup> AND M. AYGUN<sup>b</sup>

<sup>a</sup>*Bitlis Eren University, Vocational School of Technical Sciences, 13100, Bitlis, Turkey*

<sup>b</sup>*Bitlis Eren University, Faculty of Science and Arts,  
Department of Physics, 13100, Bitlis, Turkey*

Received: 18.12.2021 & Accepted: 17.02.2022

Doi: [10.12693/APhysPolA.141.507](https://doi.org/10.12693/APhysPolA.141.507)

\*e-mail: [zeynep.yarbasi@gmail.com](mailto:zeynep.yarbasi@gmail.com)

The aim of this study is to calculate radiation-matter interaction parameters of superalloys based on nickel, Rene 41, Rene 65, Rene 77, Rene 80, Rene 88 and Rene 95, which are characterized by leading features such as high operating temperatures, creep resistance, corrosion resistance, high heat resistance, low thermal conductivity and high strength. Materials with important mechanical properties should be tested for their ability to attenuate radiation. The radiation protection abilities of the alloys were obtained in a wide energy range by Phy-X/PSD code. The mass attenuation coefficients of the studied alloys were also calculated by XCOM and the obtained results were compared. Although the shielding parameters of the alloys were very close to each other, it was observed that Rene 80, Rene 88 and Rene 95 have the highest shielding abilities of the alloys. Fast neutron removal cross-section values of the alloys were also evaluated. Additionally, the dependency of linear attenuation coefficient, effective atomic number and half-value layer of the alloys on density were evaluated.

topics: radiation attenuation parameters, Rene alloys, Phy-X/PSD

## 1. Introduction

Superalloys based on nickel are well-known by their leading features such as high operating temperatures, corrosion resistance, creep resistance, high heat resistance, low thermal conductivity and high strength. These features are essential in aircraft and industrial gas turbines, petrochemical equipment, space vehicles, marine, rocket engines, components for nuclear power plants. At high operating temperatures, the superalloys used can be either in the form of cast, wrought and powder. Nickel-based superalloys typically contain Ni, Cr, Al, Co, Ti and small amounts of B, Zr, and C with other additions such as Mo, W, Ta, and Nb etc. [1]. Titanium (Ti) is important for high corrosion resistant. Carbon (C) makes the material resistant to high temperature, while molybdenum (Mo) and cobalt (Co) provide solid solution reinforcement. Chromium (Cr) is an essential element for oxidation resistance [2].

Superalloys with leading properties can be also used as radiation shielding materials due to their high radiation attenuating capabilities [3–6]. The materials to be used for radiation shielding must have certain properties, such as high atomic number (chemical composition), high density, and adequate thickness to absorb radiations [7]. Materials with high atomic number elements are preferred in radiation (X-ray and  $\gamma$ -ray) protection, while materials

with light atomic number elements are selected in fast neutron attenuation [8]. The efficiency of the radiation shielding material can be identified by determining radiation-matter interaction parameters, such as mass attenuation coefficient (MAC), linear attenuation coefficient (LAC), effective atomic number ( $Z_{\text{eff}}$ ), half value layer (HVL), tenth value layer (TVL), mean free path (MFP), effective electron density ( $N_{\text{eff}}$ ), effective conductivity ( $C_{\text{eff}}$ ), total electronic cross-section (ECS), total atomic cross-section (ACS) and buildup factors. The MAC value of the material describes the probability of photon interaction and hence shows the absorption potential of the material. Half value layer (HVL) and tenth value layer (TVL) are thickness related parameters used in the design and selection of any radiation attenuation material by reducing by half and one tenth the photon intensity, respectively [8]. The distance traveled by radiation between subsequent collisions in the material is called MFP. For higher shielding capacity, HVL, TVL and MFP with a lower values are preferred. The effective atomic number, i.e., the average atomic number of the material, is used to calculate the energy absorption and build-up factor when designing radiation shield. The buildup factor is important in radiation shielding design and dosimetry applications.

XCOM [9], WinXCom [10, 11], XMuDat [12], Geant4 [13] are well-known programs used for the determination of radiation protection parameters.

Phy-X/PSD [14], Py-MLBUF [15] and EpiXS [16] are the recently developed codes for calculating shielding parameters. The aim of this paper is to obtain the radiation attenuation parameters such as LAC, MAC,  $Z_{\text{eff}}$ , HVL, TVL, ECS, ACS,  $C_{\text{eff}}$ ,  $N_{\text{eff}}$ , fast neutron removal cross-section (FNRCs) and buildup factors of the studied alloys by using Phy-X/PSD [14]. This Phy-X/PSD software can calculate the radiation shielding parameters of materials in the range of 1 keV–100 GeV by inserting the density and chemical composition of the material. Recently, many studies about radiation shielding characteristics of materials are carried out by using this code [4–6, 17, 18]. To the best of our knowledge, the literature lacks information on the radiation protection potentials of the Rene alloys tested. Therefore, this study will be important to give comprehensive analysis about the shielding characterization of the alloys.

## 2. Materials and methods

In the study, we took the chemical compositions of Rene alloys from the literature [19–24]. Density ( $\rho_{\text{mix}}$ ) of alloys is determined by the rule of mixtures as follows [25]

$$\rho_{\text{mix}} = \left( \sum_{i=1}^n c_i A_i \right) / \left( \sum_{i=1}^n \frac{c_i A_i}{\rho_i} \right), \quad (1)$$

where  $\rho_i$ ,  $c_i$  and  $A_i$  are the density, atomic fraction and atomic weight of the  $i$ -th element, respectively.

MAC can be obtained by the Beer–Lambert as follows

$$I = I_0 e^{-\mu t}, \quad (2)$$

$$\mu_m = \frac{\mu}{\rho} = \frac{\ln(I_0/I)}{\rho t} = \frac{\ln(I_0/I)}{t_m}, \quad (3)$$

where  $\mu$  [ $\text{cm}^{-1}$ ] and  $\mu_m$  [ $\text{cm}^2/\text{g}$ ] are the linear and mass attenuation coefficients, respectively,  $t$  [cm] and  $t_m$  [ $\text{g}/\text{cm}^2$ ] are the thickness and sample mass thickness (the mass per unit area), respectively.

We can obtain the MAC for any compound as follows [26]

$$\frac{\mu}{\rho} = \sum_i w_i (\mu/\rho)_i, \quad (4)$$

where  $w_i$  and  $(\mu/\rho)_i$  are the weight fraction and the MAC of the  $i$ -th constituent element, respectively.

The total atomic cross-section ( $\sigma_a$ ) can be calculated using

$$ACS = \sigma_a = \frac{N}{N_A} \frac{\mu}{\rho}, \quad (5)$$

where  $N_A$  and  $N$  are the Avogadro's number and the atomic mass of the materials, respectively.

The total electronic cross-section ( $\sigma_e$ ) is formulated by [27]

$$ECS = \sigma_e = \frac{\sigma_a}{Z_{\text{eff}}}. \quad (6)$$

Using (5) and (6), we can find the effective atomic number,  $Z_{\text{eff}}$ , of the material as

$$Z_{\text{eff}} = \frac{\sigma_a}{\sigma_e} \quad (7)$$

and the effective electron number as

$$N_{\text{eff}} = \frac{\mu_m}{\sigma_e}. \quad (8)$$

HVL, TVL and MFP are obtained by the following formulas

$$\text{HVL} = \frac{\ln(2)}{\mu}, \quad (9)$$

$$\text{MFP} = \frac{1}{\mu}, \quad (10)$$

$$\text{TVL} = \frac{\ln(10)}{\mu}. \quad (11)$$

Effective conductivity ( $C_{\text{eff}}$ ) of materials can be given by [28]

$$C_{\text{eff}} = \frac{\rho \tau e^2 N_{\text{eff}}}{m_e} \times 10^3, \quad (12)$$

where  $m_e$  [kg] and  $e$  [C] are mass and charge of electron, respectively.

Exposure buildup factors (EBF) and energy absorption buildup factors (EABF) can be obtained by [29, 30]

$$Z_{\text{eq}} = \frac{Z_1 [\log(R_2) - \log(R)] + Z_2 [\log(R) - \log(R_1)]}{\log(R_2) - \log(R_1)}, \quad (13)$$

$$F = \frac{F_1 [\log(Z_2) - \log(Z_{\text{eq}})] + F_2 [\log(Z_{\text{eq}}) - \log(Z_1)]}{\log(Z_2) - \log(Z_1)}, \quad (14)$$

$$B(E, x) = \begin{cases} 1 + \frac{(b-1)(K^x - 1)}{K - 1} & \text{for } K = K(E, x) \neq 1, \\ 1 + (b-1)x & \text{for } K = K(E, x) = 1, \end{cases} \quad (15)$$

where

$$K(E, x) = c x^a + d \frac{\tanh\left(\frac{x}{X_k} - 2\right) - \tanh(-2)}{1 - \tanh(-2)} \quad (16)$$

for  $x \leq 40$  mfp.

The geometric progression (G-P) fitting parameters can be calculated by using values from [31] in (14). Buildup factors can be obtained using (15) by first determining  $K(E, x)$  in (16), where  $a$ ,  $b$ ,  $c$ ,  $d$  and  $X_k$  are the coefficients of G-P fitting parameters and  $x$  is thickness in mean free path (mfp).

The fast neutron removal cross-section FNRCs ( $\Sigma R$ ) values of the materials can be calculated using the following equation [26, 32]

$$\Sigma R = \sum_i \rho_i \left( \frac{\Sigma R}{\rho} \right)_i, \quad (17)$$

where  $\left( \frac{\Sigma R}{\rho} \right)_i$  is the mass removal cross-section of the  $i$ -th constituent element and  $\rho_i$  is the partial density of the material.

## 3. Results and discussion

The chemical compositions of Rene alloys were taken from literature and given in Table I [19–24]. Changes of the calculated MAC values versus photon energies (1 keV–100 GeV) are shown in Fig. 1a. At low energies, the photoelectric process is effective

TABLE I

Chemical compositions [wt%] of Rene alloys.

	Rene 41	Rene 65	Rene 77	Rene 80	Rene 88	Rene 95
C	0.04	–	0.07	0.16	0.051	0.06
Fe	3.6	1.0	0.08	0.10	–	–
Nb	–	0.7	–	0.03	0.71	3.33
Zr	–	0.05	0.01	0.04	0.045	0.06
Ni	52.92	55.43	57.08	61.88	56.61	63.05
Cr	18.6	16.0	14.61	13.4	15.74	12.9
Al	1.7	2.1	4.73	2.12	2.06	3.64
Ti	3.3	3.7	3.49	4.77	3.65	2.40
Co	10.4	13.0	15.32	9.45	12.87	7.81
Mo	9.3	4.0	4.52	4.11	4.09	3.39
W	–	4.0	–	3.92	4.16	3.35
B	–	0.016	0.015	0.02	0.015	0.01
Ta	–	–	0.05	–	–	–
S	–	–	0.001	–	–	–
Si	0.1	–	0.017	–	–	–
Mn	0.04	–	–	–	–	–
density [g/cm <sup>3</sup> ]	8.320	8.727	8.071	8.708	8.767	8.639

and MAC values decreased with increasing energy. At mid-energies, Compton scattering mainly affects MAC changes. At energies higher than 5 MeV, the MAC values increased with increasing energy by pair production process. The MAC values were also determined by XCom — a widely used code. As seen in Fig. 1a, the values calculated by XCom and Phy-X/PSD are in good agreement. Although the obtained MAC values of the Rene alloys are very close to each other, the lowest MAC values (up to 0.8 MeV) are determined for Rene 77. The same values are observed at energies greater than 0.8 MeV. The MAC values of the Rene alloys and previously reported superalloys are given in Table II.

The parameter of LAC depends on both the MAC and the density of compound. The dependence of the calculated LAC values versus photon energies (1 keV–100 GeV) is shown in Fig. 1b. Although the LAC values of the alloys are very close to each other for the energies given, Rene 77 (with the lowest density) has the lowest LAC value among them.

ACS and ECS are known as the probability of interaction per atom and per electron in a unit volume of any material, respectively. An alloy with higher ACS and ECS values can be known as a better shielding alloy. The change of the ACS and ECS values as a function of the energy of the incident photon are given in Fig. 2a and b, respectively. With increasing photon energy, the ACS and ECS values of the studied alloys decrease proportionally to the decrease in the probability of photon–atom interaction [33]. According to the obtained results for ACS and ECS parameters of the samples, Rene 77 has the lowest ACS and ECS values. The other alloys have very close values.

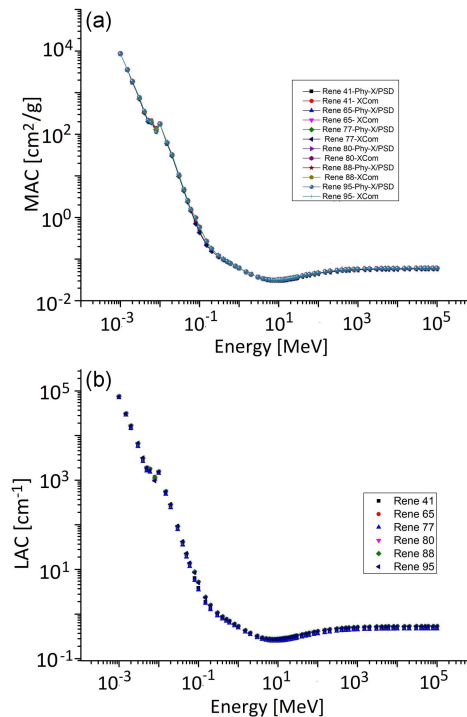


Fig. 1. The variations of MAC (a) and LAC (b) versus photon energies.

The penetration ability of the radiation in materials is given by the HVL and TVL parameters. MFP is the average distance that the radiation takes between subsequent collisions in a material. The change of the HVL, TVL and MFP parameters depending on the incident photon energies are shown in Fig. 3a–c. Alloys with lower HVL, TVL and MFP values in the high energy regions have

MAC values of Rene alloys and some superalloys.

TABLE II

Energy [MeV]	Rene 41	Rene 65	Rene 77	Rene 80	Rene 88	Rene 95	In 625 [6]	In 718 [6]	WI-52 [6]
0.015	58.48	63.59	59.63	64.38	63.88	63.06	65.70	59.00	66.24
0.03	10.69	10.45	9.734	10.44	10.52	10.83	9.549	10.41	9.830
0.05	2.594	2.540	2.351	2.537	2.558	2.633	2.287	2.51	2.412
0.8	0.068	0.068	0.068	0.068	0.068	0.068	0.068	0.067	0.068
1	0.060	0.061	0.061	0.061	0.061	0.061	0.061	0.060	0.060
3	0.037	0.037	0.037	0.037	0.037	0.037	0.037	0.037	0.036
5	0.032	0.032	0.032	0.033	0.033	0.033	0.032	0.032	0.032
8	0.031	0.031	0.031	0.031	0.031	0.032	0.031	0.031	0.031
10	0.031	0.031	0.031	0.031	0.031	0.031	0.031	0.031	0.031

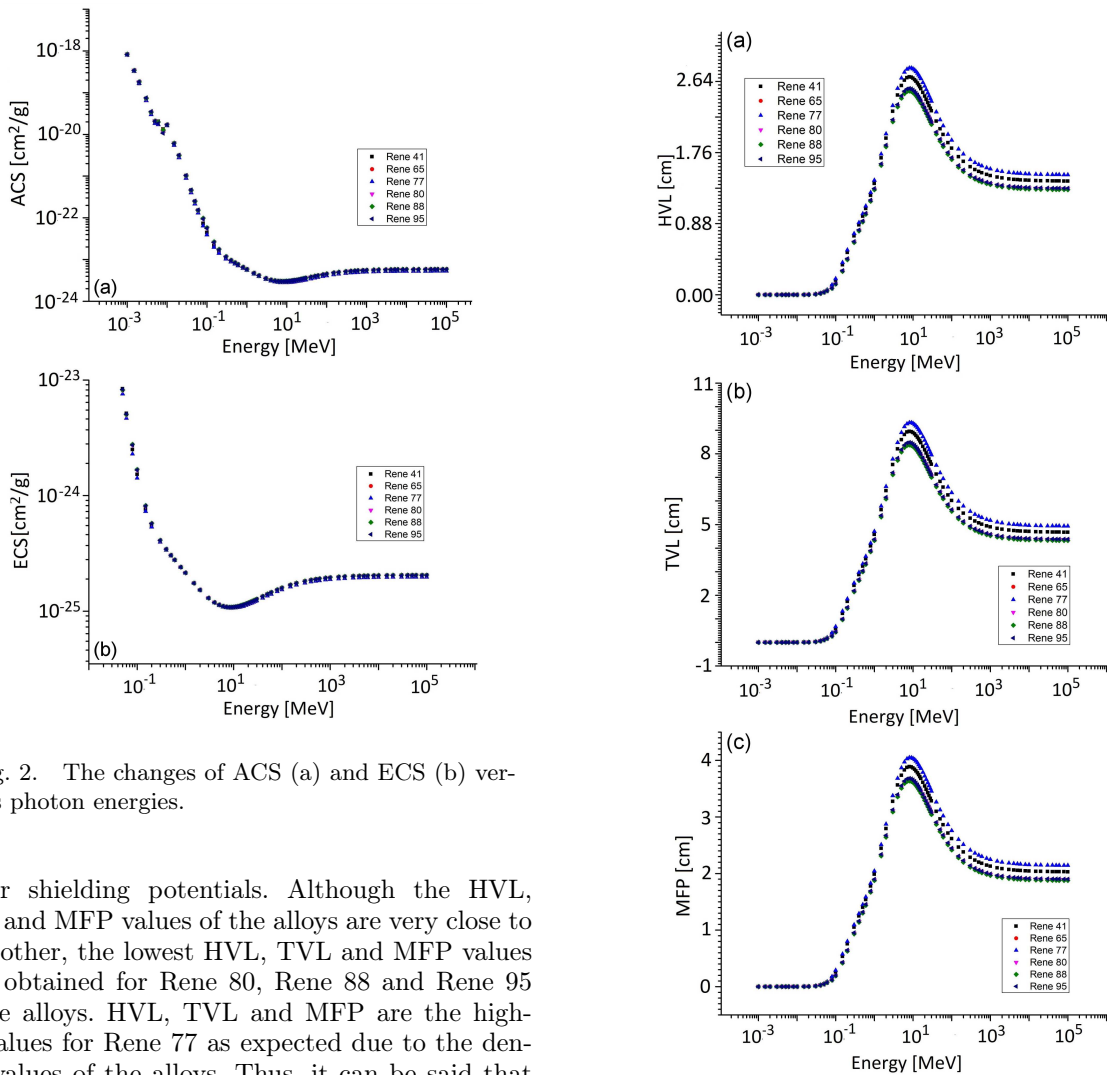


Fig. 2. The changes of ACS (a) and ECS (b) versus photon energies.

better shielding potentials. Although the HVL, TVL and MFP values of the alloys are very close to each other, the lowest HVL, TVL and MFP values were obtained for Rene 80, Rene 88 and Rene 95 of the alloys. HVL, TVL and MFP are the highest values for Rene 77 as expected due to the density values of the alloys. Thus, it can be said that Rene 80, Rene 88 and Rene 95 are better for the photon shielding abilities. Additionally, the radiation shielding abilities of Rene alloys relative to other radiation shields were evaluated by comparing the HVL values with other shielding concretes (ordinary, steel–magnetite and barite) in order to see the advantage of the thickness of the studied alloys in radiation shielding [34, 35]. The photon shielding effectiveness of Rene alloys by HVL values are shown

Fig. 3. The variations of HVL (a) TVL (b) and MFP (c) versus photon energies.

in Fig. 4 at 100 keV, 1 MeV, 100 MeV and 100 GeV. Obviously, it can be seen that the obtained HVL values of the studied alloys are lower than those of the widely used traditional shielding concretes.

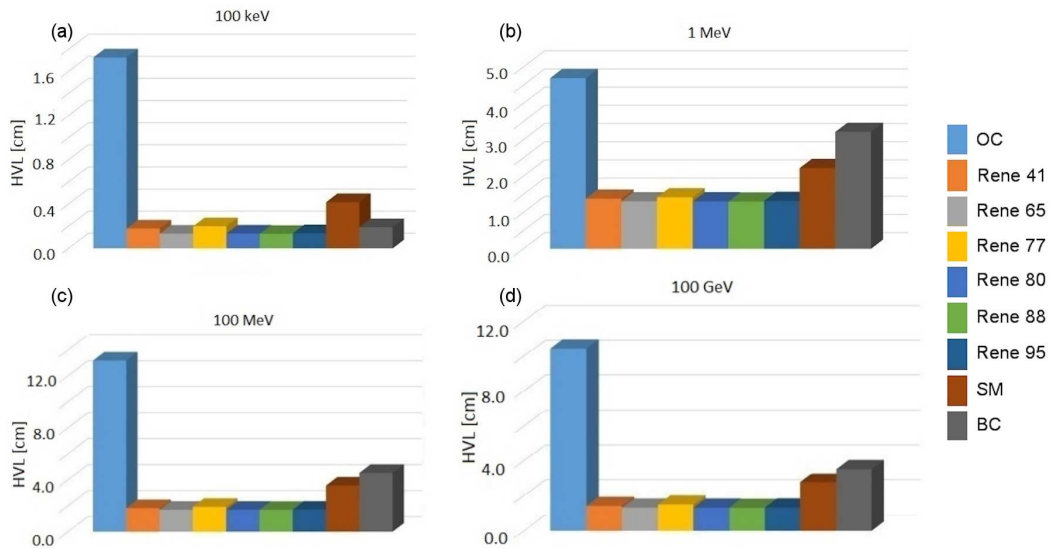


Fig. 4. The HVL values of the studied alloys and concretes (ordinary, steel-magnetite and barite).

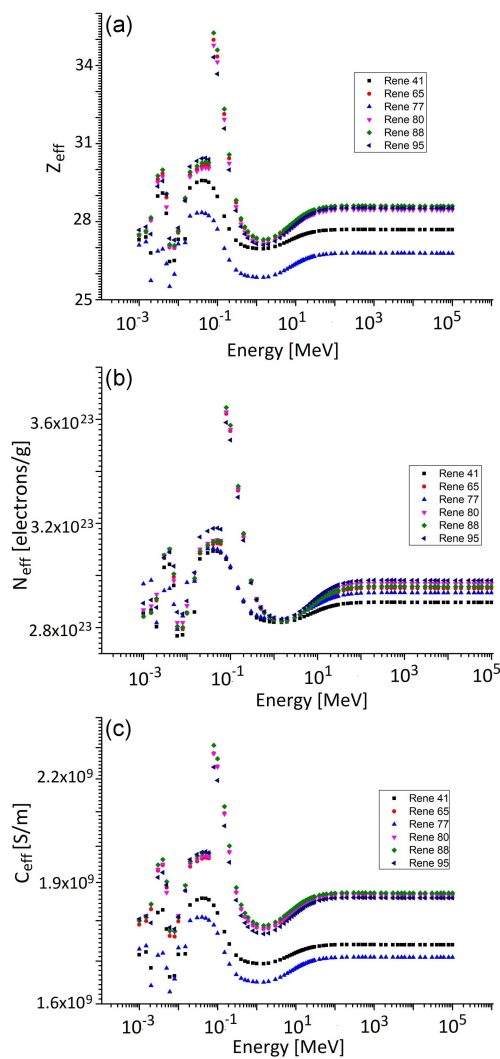


Fig. 5. The variations of  $Z_{\text{eff}}$  (a)  $N_{\text{eff}}$  (b) and  $C_v$  (c) versus photon energies.

The dependence of  $Z_{\text{eff}}$  versus energy is given in Fig. 5a. In the low-energy region, due to the photoelectric effect (photoelectric cross-section with  $Z^{4-5}$ ), the maximum  $Z_{\text{eff}}$  values were obtained. With increasing energy, these values decreased sharply due to photoelectric cross-section, proportional to  $E^{-3.5}$ . Then the values gradually increased and remained constant in high energies based on the cross-section of the pair production varying as  $Z^2$  [6]. The atomic numbers of elements of the compositions are decisive for the values of  $Z_{\text{eff}}$ . Alloys consisting of many elements with large differences in atomic numbers have the values of  $Z_{\text{eff}}$  with greater fluctuations than other studied alloys [33]. For the studied alloys, this case can be observed. Among Rene alloys, the maximum  $Z_{\text{eff}}$  values are observed for Rene 65, Rene 80, Rene 88 and Rene 95 with contribution of W, Nb, Mo, and Zr (higher atomic number); whereas the minimum  $Z_{\text{eff}}$  values are observed for Rene 41 and Rene 77 with no contribution of Nb and W. It is therefore concluded that the most obvious effect on the increase of the  $Z_{\text{eff}}$  value is the presence of the W content in the alloys. Due to the higher  $Z_{\text{eff}}$  values of Rene 80, Rene 88 and Rene 95 than those of other alloys, it can be said that Rene 80, Rene 88 and Rene 95 have higher shielding potentials.

The dependence of  $N_{\text{eff}}$  versus energy is given in Fig. 5b. As one can see, the values of  $N_{\text{eff}}$  of Rene 95 are higher than those of others, while the lowest  $N_{\text{eff}}$  is obtained for Rene 41. The parameter  $C_{\text{eff}}$ , which corresponds to the number of free electrons resulting from the photon-matter interaction is directly proportional to the effective electron densities and densities of the materials. The number of free electrons in the material depends on the photon energy by the photoelectric effect, Compton scattering and pair production interactions. The values

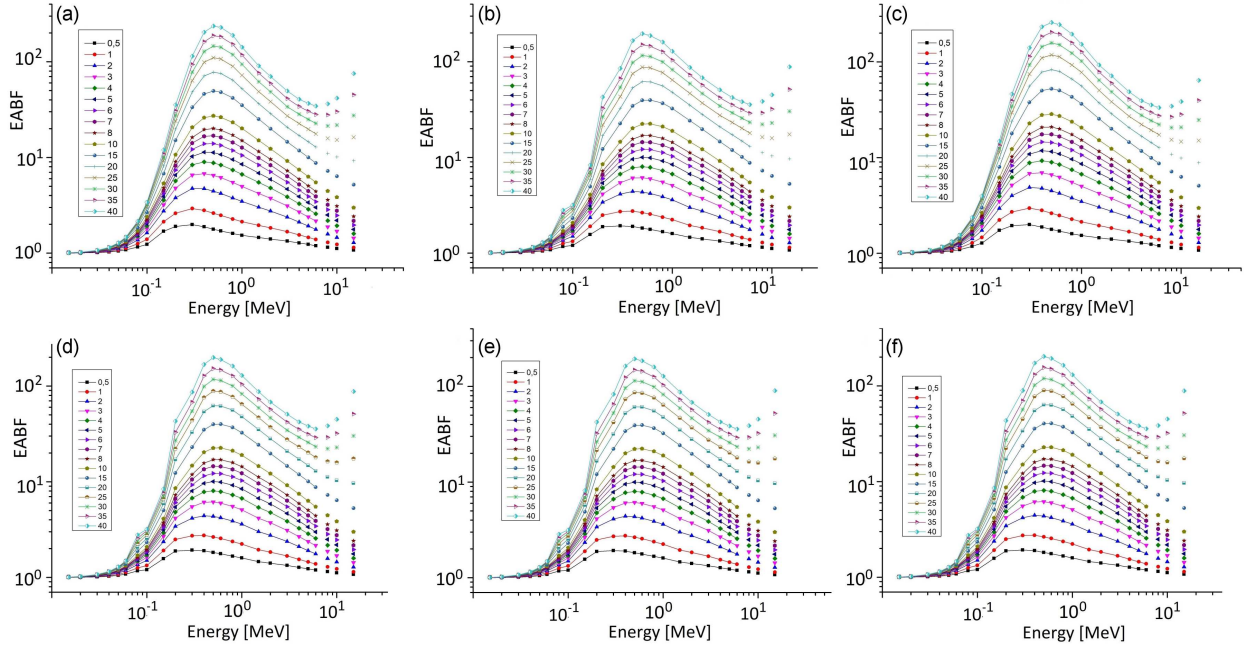


Fig. 6. The changes of EABF for Rene 41 (a) Rene 65 (b) Rene 77 (c) Rene 80 (d) Rene 88 (e) Rene 95 (f) versus photon energies.

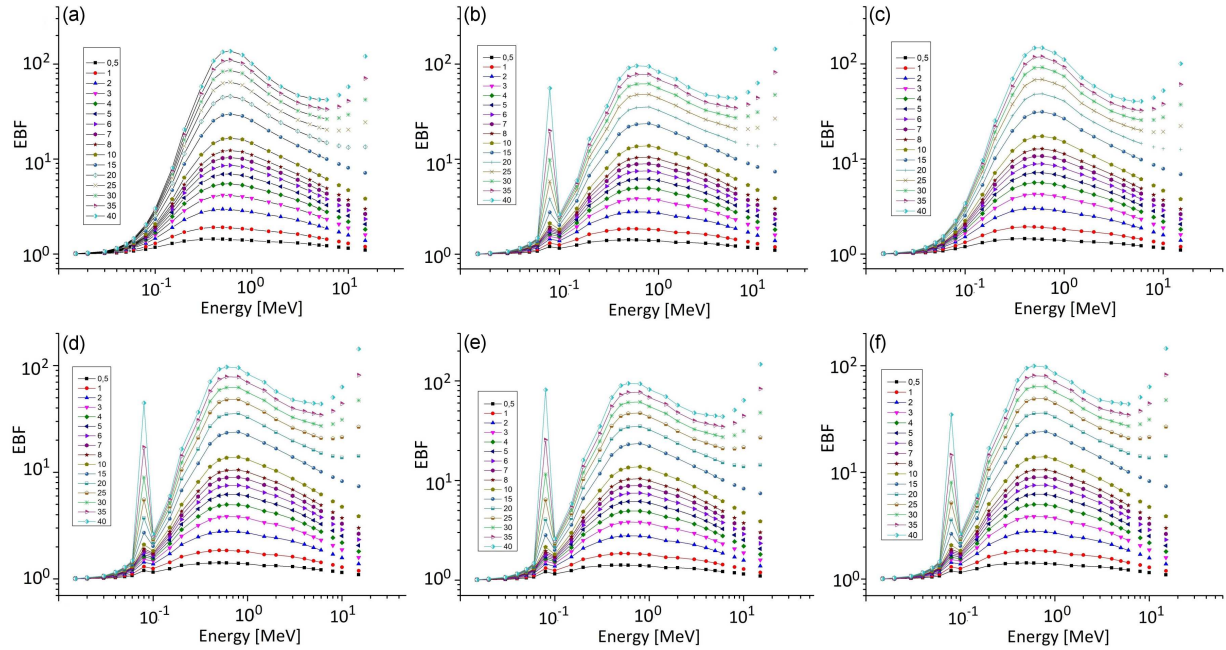


Fig. 7. The changes of EBF for Rene 41 (a) Rene 65 (b) Rene 77 (c) Rene 80 (d) Rene 88 (e) Rene 95 (f) versus photon energies.

of  $C_{\text{eff}}$  are directly proportional to the  $N_{\text{eff}}$  values, but the order of the  $C_{\text{eff}}$  and  $N_{\text{eff}}$  values of the alloys with energy is not the same due to the different densities of the alloys [33]. The dependence of  $C_{\text{eff}}$  values versus photon energies (Fig. 5c) showed that the  $C_{\text{eff}}$  values of Rene 88 is higher than those of other studied alloys due to the higher density of the alloy.

Changes of EBF and EABF versus the incident photon energies in the range  $10-10^4$  keV are shown in Figs. 6 and 7. Buildup factor values are small at low energies due to the photoelectric effect. EBF and EABF reach the maximum at mid-energies due to the large number of scattered photons as a result of the Compton process. An effective process at high energies is the pair production, thus photon

TABLE III

The values of  $Z_{eq}$  of Rene alloys.

Energy [MeV]	$Z_{eq}$					
	Rene 41	Rene 65	Rene 77	Rene 80	Rene 88	Rene 95
0.01	26.36	26.56	26.40	26.66	26.58	26.56
0.015	26.35	27.17	26.41	27.25	27.22	27.06
0.02	28.27	28.15	27.39	28.12	28.21	28.43
0.03	28.48	28.29	27.52	28.26	28.36	28.60
0.04	28.58	28.38	27.59	28.34	28.45	28.70
0.05	28.65	28.45	27.63	28.40	28.52	28.77
0.06	28.70	28.50	27.67	28.45	28.57	28.83
0.08	28.77	31.88	27.76	31.78	32.05	31.66
0.1	28.82	32.20	27.80	32.09	32.38	31.94
0.15	28.90	32.71	27.87	32.59	32.90	32.39
0.2	28.95	33.05	27.91	32.93	33.25	32.69
0.3	29.02	33.49	27.96	33.36	33.70	33.08
0.4	29.06	33.77	28.00	33.64	33.99	33.33
0.5	29.08	33.97	28.01	33.83	34.18	33.49
0.6	29.09	34.09	28.03	33.95	34.30	33.60
0.8	29.11	34.22	28.04	34.09	34.44	33.73
1	29.11	34.27	28.04	34.13	34.49	33.77
1.5	28.73	33.02	27.70	32.89	33.22	32.60
2	28.27	30.98	27.29	30.89	31.15	30.76
3	27.97	29.55	27.05	29.48	29.68	29.48
4	27.89	29.16	26.99	29.10	29.27	29.14
5	27.85	28.98	26.95	28.92	29.09	28.97
6	27.83	28.86	26.92	28.80	28.96	28.86
7	27.81	28.79	26.91	28.74	28.89	28.80
8	27.80	28.76	26.90	28.71	28.86	28.77
9	27.79	28.73	26.90	28.68	28.83	28.74
10	27.78	28.69	26.89	28.65	28.79	28.71

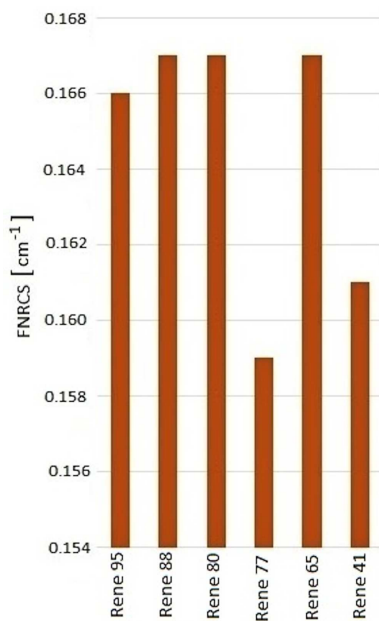


Fig. 8. FNRCs values of Rene alloys.

absorption is strongly observed, and the buildup factors decrease in this region [36, 37]. It can be said that the buildup effect is dominant at mid-energies. The EBF and EABF values reach high levels at higher MFP values due to the increased probability of photon scattering with increasing penetration depth. As with  $Z_{eff}$ , the increase observed at 0.08 MeV for EBF of Rene 65, Rene 80, Rene 88 and Rene 95 is thought to be affected by the  $K$ -absorption edge of W (tungsten) [38]. According to the obtained EABF and EBF values, the photons for Rene 65, Rene 80, Rene 88 and Rene 95 cluster less than for the others. As a result, it can be said that the Compton scattering effect is significantly observed for Rene 41 and Rene 77. It can be also said that the alloys with higher  $Z_{eff}$  have lower values for EBF and EABF, hence there is an inverse relation between EBF, EABF and  $Z_{eff}$ .

Equivalent atomic number ( $Z_{eq}$ ) is the parameter to determine the energy absorption and absorbed dose. Compton scattering is the only effective process for the  $Z_{eq}$  determination [36]. The variations of calculated  $Z_{eq}$  of the alloys are given in Table III.

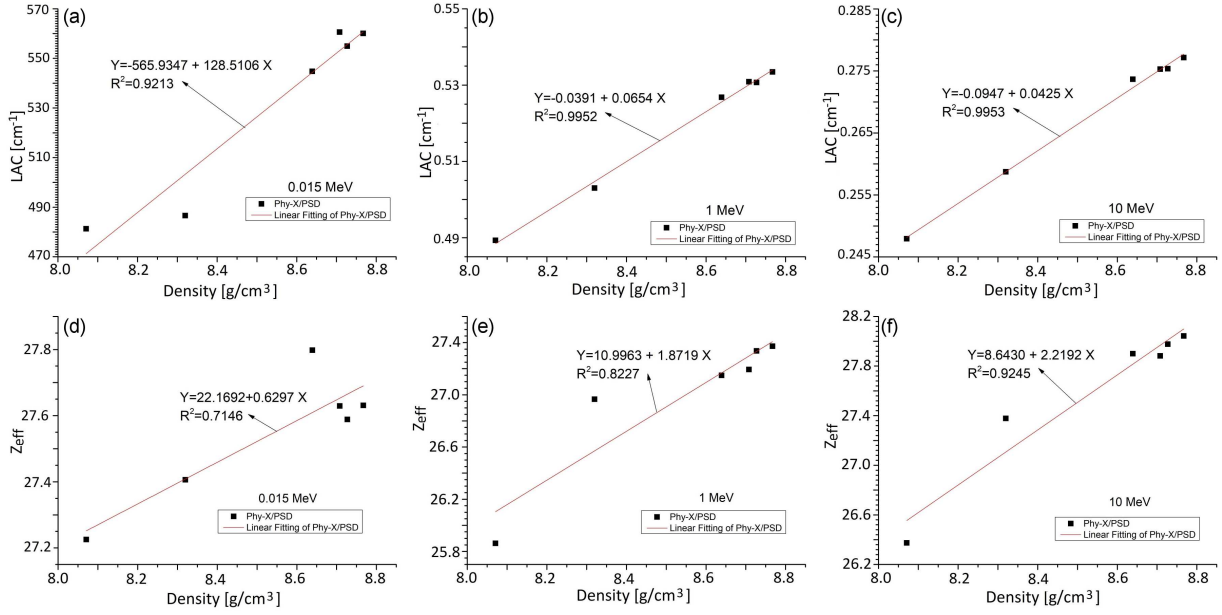


Fig. 9. Dependency of LAC and  $Z_{\text{eff}}$  of the alloys on density by Phy-X/PSD for 0.015, 1 and 10 MeV.

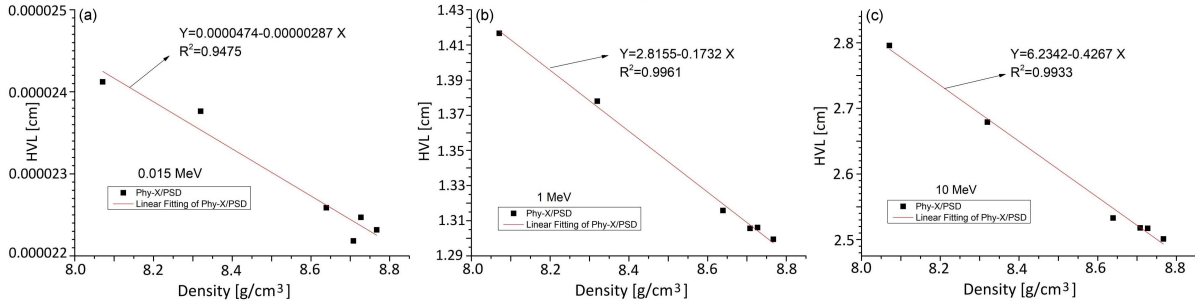


Fig. 10. Dependency of HVL of the alloys on density by Phy-X/PSD for 0.015, 1 and 10 MeV.

Alloys composed of many elements with large differences in atomic numbers have values of  $Z_{\text{eq}}$  with energy-dependent fluctuations, as observed for the  $Z_{\text{eff}}$ ,  $N_{\text{eff}}$  and  $C_{\text{eff}}$  parameters.

Fast neutron attenuation abilities of the alloys were also determined by Phy-X/PSD. The results of the fast neutron removal cross-section (FNRCs) of the studied Rene alloys are given in Fig. 8. The lowest FNRCs is observed for Rene 77 and it can be said that, apart from Rene 41 and Rene 77, other studied alloys are more appropriate for neutron shielding.

In addition to the above reviews, the dependency of the selected parameters, the linear attenuation coefficient, the effective atomic number and the alloy half value layer on density were evaluated. For the purpose of this evaluation, energy values of 0.015, 1 and 10 MeV were chosen and the dependency is shown in Figs. 9 and 10. It is found that the variation of Phy-X/PSD results of alloys with a density for different photon energies can be expressed by linear regression equations with a well-

fitted correlation coefficient  $R^2$ . The LAC and  $Z_{\text{eff}}$  values increase with increasing density for energies 0.015, 1 and 10 MeV, while HVL values decrease with increasing alloy density.

#### 4. Conclusions

In the study, radiation-matter interaction parameters of Rene alloys were determined using Phy-X/PSD code in the range of 1 keV–100 GeV in order to determine the radiation protection capabilities. According to the obtained results, although the parameter values of the studied alloys are close to each other, Rene 80, Rene 88 and Rene 95 have the highest shielding abilities among the studied alloys. Alloys with high amounts of heavy elements such as W, Nb, Mo and Zr show higher shielding property, while alloys with light elements (Si, B and S) show lower shielding property. It is also obvious that the HVL values of the studied alloys are lower than those of traditional concretes such as ordinary, steel–magnetite and barite. Additionally, depending

on the obtained FNRC values, Rene 65, Rene 80, Rene 88 and Rene 95 are more suitable for neutron shielding than Rene 41 and Rene 77. As a result, it can be stated that the studied Rene alloys can be evaluated as shielding materials with their high operating temperatures, corrosion resistance, high heat resistance, high strength features.

### References

- [1] W. Fan, W. Ji, L. Wang, L. Zheng, Y. Wang, *Int. J. Adv. Manuf. Technol.* **110**, 2863 (2020).
- [2] H. Us, Ph.D. Thesis, University of Missouri, 2016.
- [3] T. Korkut, B. Aygün, O. Bayram, A. Karabulut, *J. Radioanal. Nucl. Chem.* **306**, 119 (2015).
- [4] F. I. El-Agawany, N. Ekinçi, K.A. Mahmoud, S. Saritas, B. Aygün, E.M. Ahmed, Y.S. Rammah, *Eur. Phys. J. Plus* **136**, 527 (2021).
- [5] B. Aygün, *Radiat. Phys. Chem.* **188**, 109630 (2021).
- [6] M.I. Sayyed, F.Q. Mohammed, K.A. Mahmoud, E. Lacomme, K.M. Kaky, M.U. Khandaker, M.R.I. Faruque, *Appl. Sci.*, **10**, 7680, (2020).
- [7] T. Kaur, J. Sharma, T. Singh, *Prog. Nucl. Energy* **113**, 95 (2019).
- [8] A. Levet, E. Kavaz, Y. Özdemir, *J. Alloys Comp.* **819**, 152946 (2020).
- [9] M.J. Berger, J.H. Hubbell, S.M. Seltzer, J. Chang, J.S. Coursey, R. Sukumar, D.S. Zucker, K. Olsen *XCOM: Photon Cross Sections Database 8*, 1987.
- [10] L. Gerward, N. Guilbert, K.B. Jensen, H. Levring, *Radiat. Phys. Chem.* **60**, 23 (2001).
- [11] L. Gerward, N. Guilbert, K.B. Jensen, H. Levring, *Radiat. Phys. Chem.* **71**, 653 (2004).
- [12] R. Nowotny, *XMudat: Photon attenuation data on PC*, IAEA Report IAEA-NDS-195, 1998.
- [13] S. Agostinelli, J. Allison, K. Amako et al., *Nucl. Inst. Methods Phys. Res. A* **506**, 250 (2003).
- [14] E. Sakar, Ö.F. Özpolat, B. Alm, M.I. Sayyed, M. Kurudirek, *Radiat. Phys. Chem.* **166**, 1 (2020).
- [15] K.S. Mann, S.S. Mann, *Ann. Nucl. Energy* **150**, 107845 (2021).
- [16] F.C. Hila, A.A. Astronomo, C.A.M. Dingle et al., *Radiat. Phys. Chem.* **182**, 109331 (2021).
- [17] Z. Aygun, M. Aygun, *Karaelmas J. Sci. Eng.* **11**, 165 (2021).
- [18] U. Gökmen, *Nucl. Engineer. Tech.* **54**, 1049 (2021).
- [19] E. Ungureanu (Arva), D.C. Anghel, D. Negrea, A.G. Plaiasu, V. Rizea, M.M. Dicu, C.M. Ducu, M. Abrudeanu, *IOP Conf. Ser. Mater. Sci. Eng.* **564**, 012046 (2019).
- [20] J.A. Heaney, M.L. Lasonde, A.M. Powell, B.J. Bond, C.M. O'Brien, in: *Proc. of the 8th Int. Symposium on Superalloy 718 and Derivatives*, Ed. U. John, Wiley & Sons, Inc., Hoboken (NJ) 2014, p. 67.
- [21] M. Zielińska, J. Sieniawski, B. Gajecka, *Arch. Foundry Eng.* **9**, 221 (2009).
- [22] M. Aghaie-Khafri, S. Farahany, *J. Mater. Eng. Perform.* **19**, 1065 (2010).
- [23] Y.K. Cho, D.Y. Yoon, M.F. Henry, *Metall. Mater. Trans. A* **32A**, 3077 (2001).
- [24] W.M. Kane, U. Krupp, T. Jacobs, C.J. McMahon, *Mater. Sci. Eng. A* **402**, 42 (2005).
- [25] C. Xiang, E.H. Han, Z.M. Zhang, H.M. Fu, J.Q. Wang, H.F. Zhang, G.D. Hu, *Intermetallics* **104**, 143 (2019).
- [26] E. Şakar, *Radiat. Phys. Chem.* **172**, 1 (2020).
- [27] I. Han, L. Demir, *Nucl. Instrum. Methods B* **267**, 3 (2009).
- [28] H.C. Manjunatha, *Radiat. Phys. Chem.* **137**, 254 (2017).
- [29] Y. Harima, Y. Sakamoto, S. Tanaka, M. Kawai, *Nucl. Sci. Eng.* **94**, 24 (1986).
- [30] Y. Harima, *Radiat. Phys. Chem.* **41**, 631 (1993).
- [31] D.K. Trubey, C.M. Eisenhauer, A. Foderaro, D.V. Gopinath, Y. Harima, J.H. Hubbell, K. Shure, S.-. Su "Gamma-ray Attenuation Coefficients and Buildup Factors for Engineering Materials", ANSI/ANS- 6.4.3, American Nuclear Society, La Grange Park (IL) 1991.
- [32] J. Wood, *Computational Methods in Reactor Shielding*, Elsevier, 2013.
- [33] B. Alm, *Appl. Phys. A* **126**, 262 (2020).
- [34] I.I. Bashter, *Ann. Nucl. Energy* **24**, 1389 (1997).
- [35] K.J. Singh, N. Singh, R.S. Kaundal, K. Singh, *Nucl. Inst. Methods Phys. Res. B* **266**, 944 (2008).
- [36] Z. Aygun, M. Aygun, *Int. J. Environ. Sci. Technol.* (2021).
- [37] Z. Aygun, N. Yarbasi, M. Aygun, *Ceram. Int.* **47**, 34207 (2021).
- [38] M.S. Al-Buriah, T.A. Taha, M.A. Alothman, H. Donya, I.O. Olarinoy, *Eur. Phys. J. Plus* **136**, 779 (2021).